Chapter 1

Sandy beach dynamics by constrained wave energy minimization

This chapter focuses on a new approach to describe coastal morphodynamics, based on optimization theory, and more specifically on the assumption that a sandy beach profile evolves in order to minimize a wave-related function, the choice of which depends on what is considered the driving force behind the coastal morphodynamic processes considered. The numerical model derived from this theory uses a gradient descent method and allows us to account for physical constraints such as sand conservation in wave flume experiments. Hence, the model automatically adapts to either wave flume or open sea settings and only involves two hyper-parameters: a sand mobility and a critical angle of repose. The ability of OptiMorph to model cross-shore beach morphodynamics is illustrated on a flume configuration. Comparison of the beach profile changes computed with OptiMorph with experimental data as well as the results from the coastal morphodynamic software XBeach demonstrates the potential of a model by wave energy minimization. Numerical robustness and a multi-1D extension are also discussed.

Current chapter contents

1 Introduction

Optimization theory is the study of the evolution of a system while searching systematically for the minimum of a function derived from physical properties of the system. In this chapter, we have applied this approach to coastal dynamics, with our primary objective to simulate the interactions between the waves and the sea bottom along a cross-shore profile. Using mathematical optimization theory (Isèbe et al. 2014; Isèbe et al. 2008b; Isèbe et al. 2008a; Bouharguane et al. 2010; Mohammadi et al. 2014; Mohammadi et al. 2011; Cook et al. 2021c; Mohammadi 2017; Bouharguane et al. 2012), we have designed a model that describes the evolution of the sea bottom while taking into account the coupling between morphodynamic and hydrodynamic processes. This study focuses on a theoretical and numerical approach to the modeling of this coupling, based on the assumption that the beach profile adapts to minimize a certain wave-related function. The choice of this function determines the driving force behind the morphological evolution of the beach profile. This optimization problem is subjected to a certain number of constraints, allowing for a more accurate description of the morphodynamic evolution. This study is accompanied by the development of a numerical hydro-morphodynamic model, which has the advantages of being fast, robust, and of low complexity. The model was given the name *OptiMorph*.

The chapter starts with a description of the simple hydrodynamic model used to calculate the driving forces behind the morphodynamic processes. Then, we provide a description of the morphodynamic model (OptiMorph) based on wave-energy minimization. With the purpose of validating OptiMorph, we compare the results of the numerical simulation with that of experimental data acquired in a flume experiment. We also compared the model to another nearshore hydro-morphodynamic model, XBeach (D. J. Roelvink et al. 2009), to see how it fares against existing hydro-morphodynamic models, XBeach being considered to be quite a reputable model in the coastal dynamic community (Zimmermann et al. 2012; Bugajny et al. 2013; Williams et al. 2015).

1.1 State of the Art

Numerical models of morphodynamic processes are seen as a valuable tool for understanding and predicting the evolution of the sediment transport of the morphology over time in coastal areas. Different morphodynamic models exist in the literature, ranging from empirical models (Vriend et al. 1994; Gravens 1997; Kana et al. 1999; Ruessink et al. 2000) to process-based models. The latter can be sorted into several categories, such as i) profile evolution models (Larson et al. 1989; Larson et al. 1990; Nairn et al. 1993), which use only cross-shore transport, ii) rules-based models (Storms et al. 2002; McCarroll et al. 2021), based on a number of rules such as Brunn's rule (Bruun 1954), iii) 2D morphological models (Fleming et al. 1977; Latteux 1980; Coeffe et al. 1982; Yamaguchi et al. 1985; Watanabe et al. 1986; Maruyama et al. 1988; Wang et al. 1993; Johnson et al. 1995; Nicholson et al. 1997; D. J. Roelvink et al. 2009), which use depth-averaged wave and current equations to model the sediment transport while neglecting the vertical variations of wave-derived parameters, as well as iv) 3D and quasi-3D models (J. A. Roelvink et al. 1994; Lesser et al. 2004; D. J. Roelvink et al. 1995; Briand et al. 1993; Zyserman et al. 2002; Ding et al. 2006; Droenen et al. 2007), which determine the sediment evolution using both horizontal and vertical variations of the wave-derived parameters.

The OptiMorph model described in this chapter is based on optimal control. In the past, the use of optimization theory has primarily been used in the design of coastal defense structures, whether in the design of ports and offshore breakwaters (Isèbe et al. 2008b; Isèbe et al. 2008a).

Optimal control has already been considered for the modeling of shallow water morphodynamics, based on the assumption that the seabed acts as a flexible structure and adapts to a certain hydrodynamic quantity (Mohammadi et al. 2011; Bouharguane et al. 2010). These studies were based on somewhat theoretical developments with no direct relationship with real case studies. Our objectives in this work is to produce a physically robust numerical morphodynamic model based on optimal control and to validate it using numerical data from well established morphodynamics software as well as wave flume experiments.

1.2 Hypotheses

OptiMorph is based on a certain number of assumptions. First, since the model is based on the minimization of a cost function, some hypotheses must be made regarding the choice of this function. This function, which originates from a physical quantity, must be directly linked to the elevation of the seabed. In the current version of the model, we set the quantity to be minimized as the energy of shoaling waves. This implies that the sea bottom reacts to the state of the waves by minimizing the energy of shoaling waves.

Other assumptions assess the behavior of the sea bottom and originate from general observations. In particular, the bed-load sediment transport is controlled by the orbital displacement of water particles (R.L. Soulsby 1987); thus a greater sediment mobility has to be considered in shallower waters. Another natural observation concerns the slope of the seabed, which cannot be overly steep without an avalanching process occurring (Reineck et al. 1973). Last, in an experimental wave flume, the quantity of sand must remain constant over time, with no inflow or outflow of sand to alter the sand stock.

2 Numerical Model

Modeling Framework

For the sake of simplicity, we present the principle of morphodynamics by optimization in a one-dimensional setting. This enables us to compare the numerical results based on this theory with experimental flume data. However, no assumptions are made regarding the dimension of the problem, and as a result, it is straightforward to extend this theory to a two-dimensional configuration.

We consider a coordinate system composed of a horizontal axis x and a vertical axis z. We denote $\Omega := [0, x_{\max}]$ the domain of the cross-shore profile of the active coastal zone, where $x = 0$ is a fixed point in deep water where no significant change in bottom elevation can occur, and $x_{\max}$ is an arbitrary point at the shore beyond the shoreline, as shown by Figure 1.1. The elevation of the sea bottom is a one-dimensional positive function, defined by: $\psi : \Omega \times [0, T_f] \times \Psi \to \mathbb{R}^+$ where $[0, T_f]$ is the duration of the simulation (s) and Ψ is the set of physical parameters describing the characteristics of the beach profile. In order to model the evolution over time of ψ and given the assumption that ψ changes over time in response to the energy of shoaling waves, a description of the surface waves is needed.

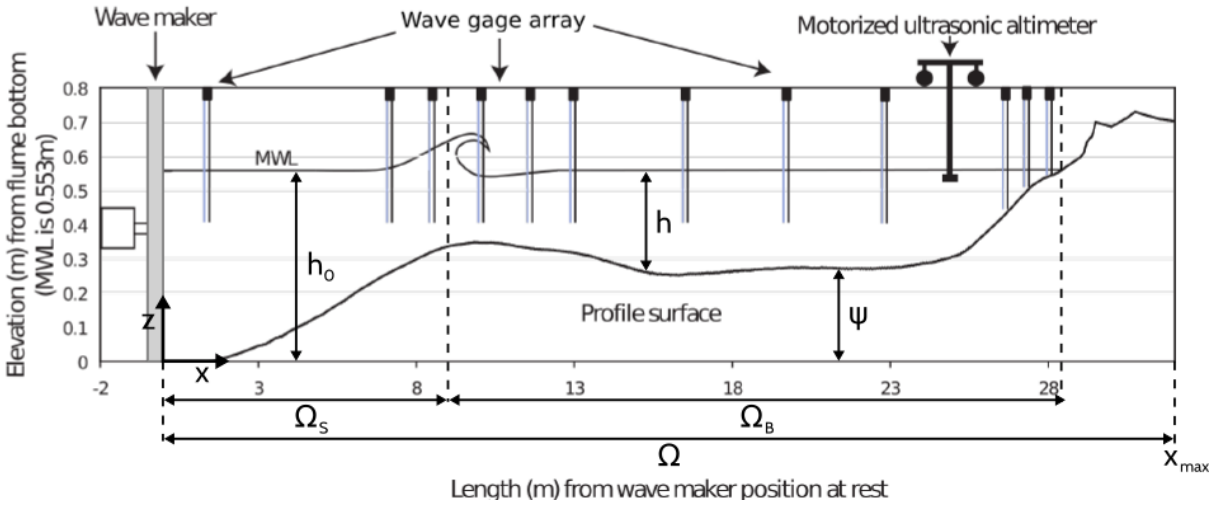

Figure 1.1 – Diagram of a cross-shore profile in the case of an experimental flume.

The model developed by Cook (2021) *et al* is based on the principle that nature tries to minimize the energy it spends. This time, the $\mathcal{J}$ cost function that governs the evolution of the ocean floor is a representative quantity of $\mathcal{E}_{\mathcal{H}}$, the energy of the waves. The model is based on the following workflow:

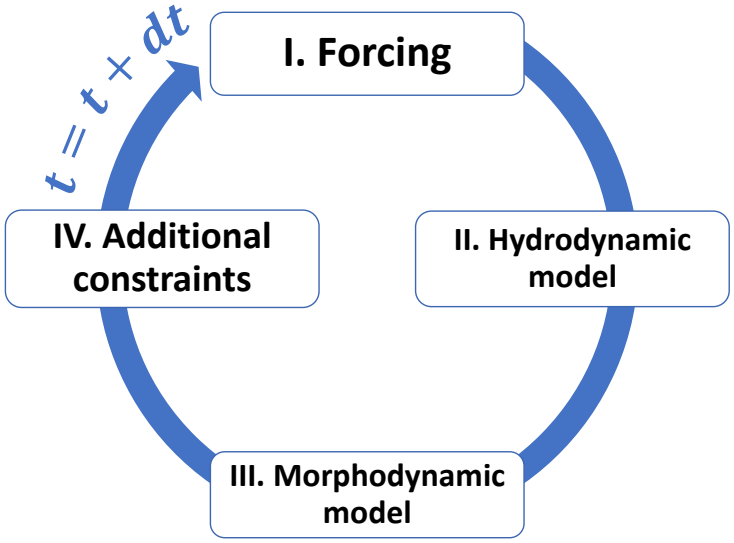

Figure 1.2 – Workflow of Optimorph 2021

with phase I. of forcing 2.1, phase II. of the hydrodynamic model 2.2, phase III. of the morphodynamic model 2.3 and the last phase IV. of constraints 2.4.

2.1 Model forcing

This hydro-morphodynamic model needs a number of forcing parameters. These very classical parameters are divided in 4 parts: numerical, geometric, hydrodynamic and morphodynamic parameters. They are presented in the table below.

Physics	Parameters	Definition
Numerical parameters	Δx	Spatial step [m]
	T_{coupl}	Coupling time between hydro and morpho [s]
	T_f	Simulation time [s]
	n_{iter}	Number of iterations
Domain	L	Domain size [m]
	h	Offshore water depth [m]
	α	Slope for a linear bathymetry
Hydrodynamic	H(t)	Offshore water height [m]
	Hmax	Maximum water depth offshore [m]
	T_0	Wave period [s]
Morphodynamic	ψ_0	Initial Sea bottom elevation
	Y	Sediment mobility [m.s.kg-1]
	β	Maximum slope

Table 1.1 – Table of different forcing parameters

These parameters are very similar to other models. However, there is an original parameter which is the sediment mobility parameter Y. This one will be used in the morphodynamic calculation. It will be defined later.

2.2 Hydrodynamic Model

The literature on hydrodynamic models is vast (Murray 2007). However, our main focus in this work is a) on the morphodynamic part of the approach and b) on providing evidence of the ability of optimization to perform robust morphodynamic prediction even under weakly constrained hydrodynamics. So we present the procedures with a hydrodynamic model as simple as possible, that is based on the linear wave theory (Dean et al. 2004), a very basic shoaling equation and some geometrical breaking parameter. It has the advantage of being easy to differentiate compared to more sophisticated models that would need automatic differentiation (Hascoet et al. 2004; Mohammadi et al. 2011) or huge additional numerical developments. This numerical implementation has a significantly short run-time as shown by the convergence results of the section 5.1. This

model has the advantage of expressing wave height as an explicit function of the bottom elevation, which leads to rapid calculations of the morphodynamics.

Let h (m) be the depth of the water from a mean water level h_0 at the point where waves are generated (cf. Figure 1.1). Ocean waves, here assumed monochromatic, are characterized by phase velocity C (m s^{-1}), group velocity C_g (m s^{-1}), and wave number k (m^{-1}), determined by the linear dispersion relation (1.1), where σ is the pulsation of the waves (s^{-1}) and g is the gravitational acceleration (m s^{-2}):

$$\sigma^2 = gk \tanh(kh) \tag{1.1}$$

We define Ω_S as the time-dependent subset of Ω over which the waves shoal and Ω_B the subset of Ω over which the waves break, cf. Figure 1.1. Munk's breaking criterion (W. Munk 1949) enables us to define $\Omega_S(t) = \left\{x \in \Omega, \frac{H(x,t)}{h(x,t)} < \gamma\right\}$ and $\Omega_B(t) = \left\{x \in \Omega, \frac{H(x,t)}{h(x,t)} \geq \gamma\right\}$, where γ is a wave breaking index. We have the model below:

Simple Shoaling model

$$H(x,t) = \begin{cases} H_0(t) Ks(x,h) & \text{for } x \in \Omega_S \quad (1.2a) \\ \gamma h(x,t) & \text{for } x \in \Omega_B \quad (1.2b) \end{cases}$$

where H is the height of the waves over the cross-shore profile, $H_0(t)$ is the deep water wave height and K_S is a shoaling coefficient, given by:

$$K_S = \left(\frac{1}{2}\frac{C_0}{C_g}\right)^{\frac{1}{2}} \tag{1.3}$$

where C_0 is the deep water wave velocity, and:

$$n = \frac{C}{C_g}, \quad C = C_0 \tanh(kh), \quad C_g = \frac{1}{2}C\left(1 + \frac{2kh}{\sinh(2kh)}\right). \tag{1.4}$$

These developments have been detailed is the section 3.This model gives us this type of height H for a linear bathymetry.

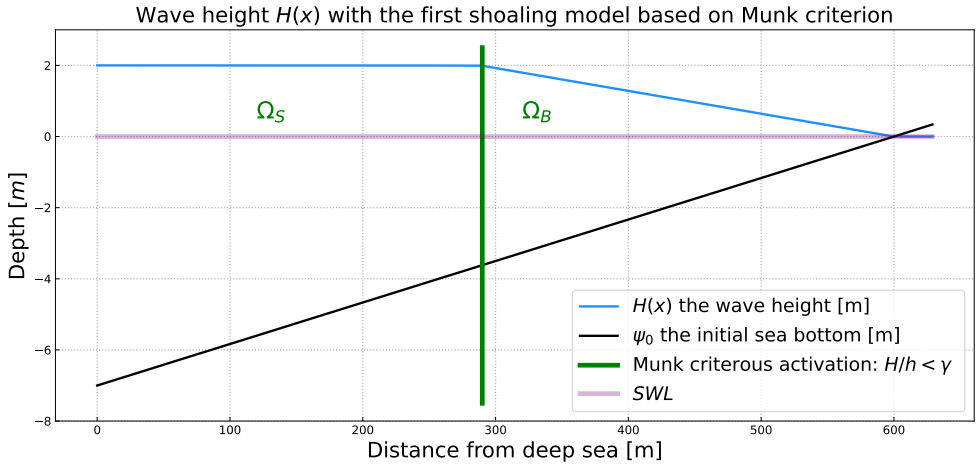

Figure 1.3 – Wave height $H(x)$ with the simple Shoaling model for a configuration with a linear bathymetry of slopes about 0.11, wave period $T_0 = 2\,s$ and offshore water height of $H_0 = 2\,m$.

Instead of considering that waves depend solely on offshore wave height H_0, this model suggests that shoaling waves are decreasingly influenced by seawards waves. The greater the distance, the less effect it has on the present wave height. As such, we introduce a weighting function w. Assuming that the maximal distance of local spatial dependency of a wave is denoted d_w, the weighting function over the maximal distance d_w is given by $w : [0, d_w] \to \mathbb{R}^+$ such that $w(0) = 1$, $w(d_w) = 0$ and decreases exponentially.

Equation (1.2a) for shoaling wave height becomes equation (1.5), where H_0^w is defined by (1.6).

$$H(x,t) = H_0^w(x,t)K_S(x,t) \tag{1.5}$$

$$H_0^w(x,t) = \frac{1}{\int_{x-X}^{x} w(x-y)\mathrm{d}y}\int_{x-X}^{x} w(x-y)H(y)K(y)\mathrm{d}y \tag{1.6}$$

Equation (1.5) applies only to the shoaling, nearshore-dependent waves of Ω_S, significant wave height over the cross-shore profile $H : \Omega \to \mathbb{R}^+$ is defined by (1.7), where $\alpha(x) = \dfrac{x}{d_w}$ over $[0, d_w]$ to allow a smooth transition between offshore and nearshore-dependent waves.

Complexified Shoaling model

$$H(x,t) = \begin{cases} [(1-\alpha(x))H_0(t) + \alpha(x)H_0^w(x,t)]\,K_S(x,t) & \text{if } x \in \Omega_S \text{ and } x < d_w \\ H_0^w(x,t)K_S(x,t) & \text{if } x \in \Omega_S \text{ and } x \geq d_w \\ \gamma h(x,t) & \text{if } x \in \Omega_B \end{cases} \tag{1.7}$$

This gives us this type of height H for a linear bathymetry.

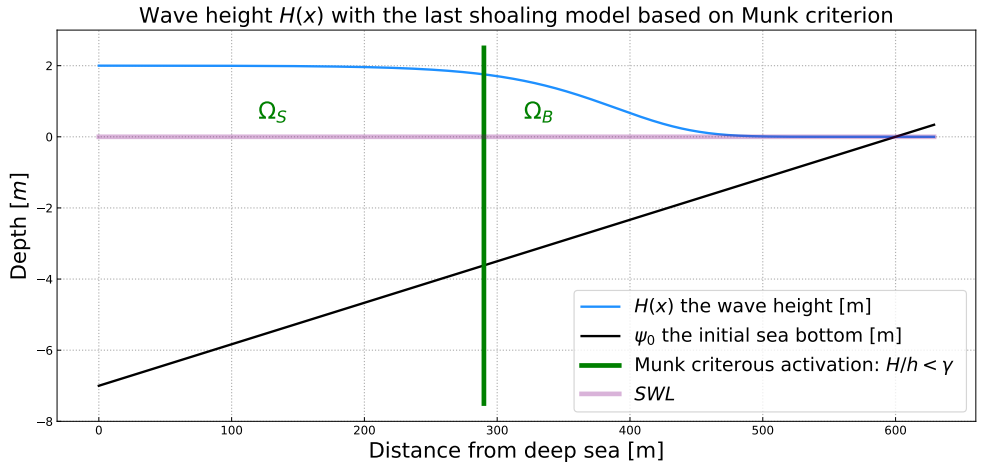

Figure 1.4 – Wave height $H(x)$ with the improved Shoaling model for a configuration with a linear bathymetry of slopes about 0.11, wave period $T_0 = 2\,s$ and offshore water height of $H_0 = 2\,m$.

2.3 Morphodynamic Model by Wave Energy Minimization

The evolution of the sea bottom is assumed to be driven by the minimization of a cost function $\mathcal{J}$ (J s m^{-1}). Recalling the hypotheses made in Section 1.2, the shape of the beach profile is determined by the minimization of the potential energy of shoaling waves, for all $t \in [0, T_f]$:

$$\mathcal{J}(\psi,t) = \frac{1}{16}\int_{t-T_{coupl}}^{t}\int_{\Omega_S} \rho_w g H^2(\psi,x,\tau)\mathrm{d}x\mathrm{d}\tau \tag{1.8}$$

where H denotes the height of the waves over the cross-shore profile (m), ρ_w is water density (kg m^{-3}), and g is the gravitational acceleration (m s^{-2}). T_{coupl} (s) defines the coupling time interval between hydrodynamic and morphodynamic models so that we

have T_f / T_{coupl} iterations. In order to describe the evolution of the beach profile, whose initial state is given by ψ_0, we assume that the sea bottom elevation ψ, in its effort to minimize $\mathcal{J}$, verifies the following dynamics:

$$\begin{cases} \psi_t = \Upsilon \, \Lambda \, d \\ \psi(t=0) = \psi_0 \end{cases} \tag{1.9}$$

where ψ_t is the evolution of the bottom elevation over time (m s^{-1}), Υ is a measure of the sand mobility expressed in m s kg^{-1}. This parameter is defined on the basis of flux-based morphodynamic models, as shown in the section **2.3.1**. It has the same functionality as XBeach's morphological factor (J.A. Roelvink 2006) where it is possible to divide simulation times by 18 as performed in (Shafiei et al. 2023; Marchesiello et al. 2022) on the LIP-1B experiment. Λ measures the excitation of the seabed by the orbital motion of water waves, and d is the direction of the descent (J s m^{-2}), which indicates the manner in which the sea bottom changes. In unconstrained configurations, there would be $d = -\nabla_\psi \mathcal{J}$, which by its definition indicates the direction of a local minimum of $\mathcal{J}$ with respect to ψ as illustrated in figure **1.5**.

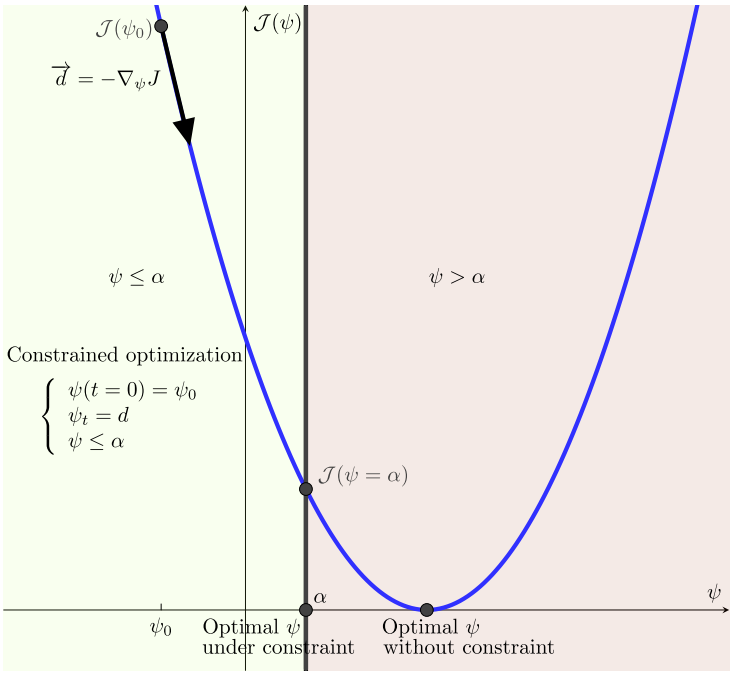

Figure 1.5 – Illustration of gradient descent with $\psi \leq \alpha$. The optimum does not necessarily correspond to the critical point $\nabla_\psi \mathcal{J} = 0$.

The approach involves two parameters with clear physical interpretation: the constraints defined in section **2.4**.

Remark: This dynamic described (eq (**5.16**)), only modifies the bottom elevation and

does not account for lateral displacements. It permits, for instance, the apparition of sedimentary bars but cannot predict their lateral displacements. This will be discussed more thoroughly in the discussion from chapter 3, section 5.2.

2.3.1 Link with Morphodynamic Flux-Based Models and Sediment Characteristics Υ

In this section, we show how to link the bed receptivity coefficient in minimization-based to the bed porosity in classical flux-based morphodynamic models. The literature on morphodynamic models is vast (Nielsen 1992; Nielsen 2002; Rooijen et al. 2012; Chen et al. 2023). Modern numerical implementations rely on models which are in a divergence form. For instance, the Exner equation (Paola et al. 2005; Yang et al. 1996) describes the conservation of mass between sediment in the bed of a channel and sediment that is being transported. It states that bed elevation increases (the bed aggregates) proportionally to the amount of sediment that drops out of transport, and conversely decreases (the bed degrades) proportionally to the amount of sediment that becomes entrained by the flow. The model involves the local porosity of the bed $\lambda_p(x) \in [0,1[$, a function in space x, but not in time. The model writes:

$$\psi_t + \frac{1}{1-\lambda_p(x)} \operatorname{div}\left(q(x,t)\right) = 0,$$

completed with initial and boundary conditions.

In the literature, the expression of q is diverse. But our discussion remains the same whatever may be the formulation of q. For the sake of simplicity, we consider q_x a flux in one dimension of space. Now, let us write the flux-based model and link it to our approach presented through the steepest descent formulation for simplicity:

$$\psi_t = -\frac{1}{1-\lambda_p(x)} q_x = -\Upsilon(x)\Lambda(x)\nabla_\psi \mathcal{J}(x,t). \tag{1.10}$$

There is no explicit boundary condition in the minimization model. In this case, we consider $\Lambda(x) = 1$, the maximum disturbance. As we saw, global sand conservation, can be evaluated through a constraint. In the same way, the local maximum slope is expressed as a constraint. $\nabla_\psi \mathcal{J}(x,t)$ corresponds to the direction of the descent without constraint and d with. The bed receptivity $\Upsilon(x)$ is a positive function which we link to the couple bed porosity $\lambda_p(x)$ and flux q as follows.
Locally integrating in space equation (1.10) over a small interval $]x-\varepsilon, x+\varepsilon[$ around x we have:

$$\int_{x-\varepsilon}^{x+\varepsilon} \Upsilon(s)\nabla_\psi \mathcal{J}(s,t)ds = \int_{x-\varepsilon}^{x+\varepsilon} \frac{1}{1-\lambda_p(s)} q_s(s,t)ds.$$

Assuming Υ and λ_p constant over this small interval, which is physically realistic, we

have:

$$\Upsilon(x)\int_{x-\varepsilon}^{x+\varepsilon}\nabla_\psi\mathcal{J}(s,t)ds=\frac{1}{1-\lambda_p(x)}\int_{x-\varepsilon}^{x+\varepsilon}q_s(s,t)ds.$$

This leads to:

$$\Upsilon(x)\int_{x-\varepsilon}^{x+\varepsilon}\nabla_\psi\mathcal{J}(s,t)ds=\frac{1}{1-\lambda_p(x)}(q(x+\varepsilon,t)-q(x-\varepsilon,t))$$

which we write as:

$$\Upsilon(x)=F(x,t)\frac{1}{1-\lambda_p(x)},$$

where factor $F(x,t)$:

$$F(x,t)=\frac{q(x+\varepsilon,t)-q(x-\varepsilon,t)}{2\varepsilon\overline{\nabla_\psi\mathcal{J}}|_{(x,t)}}$$

represents the ratio between the local flux difference and the local average shape gradient $\overline{\nabla_\psi\mathcal{J}}|_{(x,t)}=(1/(2\varepsilon))\int_{x-\varepsilon}^{x+\varepsilon}\nabla_\psi\mathcal{J}(s,t)ds$ at point x.

If the bed porosity does not change in time, this evaluation is made only once at $t=0$ and hence, given a flux and a bed porosity, the corresponding minimization-based procedure can receive an equivalent pointwise initialization (at the first iteration in an iterative time integration procedure).

In operational conditions however, it is very unlikely to have a pointwise, even inaccurate, estimation of $\lambda_p(x)$. It is more reasonable to look for an 'equivalent' constant bed porosity for a given site knowing that what is important in coastal engineering is not the knowledge of the pointwise bed porosity, but the prediction of beach future behaviour based on this site macroscopic characteristics. Also, in homogeneous bed, as it is often the case in sandy beaches, $\lambda_p(x)$ is a constant. We therefore look for a constant bed receptivity $\Upsilon=\overline{F}\frac{1}{1-\lambda_p}$ over the domain of interest $]x_L,x_R[$ (L, R indicating Left and Right) given constant bed porosity λ_p and flux q with

$$\overline{F}=\frac{q(x_R,0)-q(x_L,0)}{\int_{x_L}^{x_R}\nabla_\psi\mathcal{J}(s,0)ds},\tag{1.11}$$

which is a scalar, and the ratio between flux variation over $]x_L,x_R[$ and the average of local shape gradients. Here we have defined x_L and x_R as the Left and Right extremities of the domain. So we have $q(x_R,0)$ and $q(x_L,0)$ the boundary conditions of the flux-based model. $\overline{F}$ is a measure of how the evaluation of local-based and optimization-based fluxes differs.

2.3.1.1 Illustration using a simple model

Assuming that we are on a configuration of bed load transportation without suspended transport, we can calculate $q(x_R,0)$ and $q(x_L,0)$ by using a formula of the bed load transport rate q with (Fredsøe et al. 1992):

$$q = 10\frac{\pi}{6}d_{50}pU'_f[1-0.7\sqrt{\theta_c/\theta'}] \tag{1.12}$$

with d_{50} the grain diameter, p the fraction of bed surface particles in motion, U'_f the skin friction velocity, θ_c the critical Shields parameter and θ' the Shields parameter. This formula has been chosen as one of the simplest. However, we can choose to take suspended sediment transport into account, simply by changing the expression of q in our model. Combining the equations (**1.11**) and (**1.12**), we obtain the following expression of $\overline{F}$:

$$\overline{F} = \pi d_{50}[10-7\sqrt{\theta_c/\theta'}]\frac{p(x_L)Uf'(x_L)-p(x_R)Uf'(x_R)}{6\int_{x_L}^{x_R}\nabla_\psi \mathcal{J}(s,0)ds}.$$

We have shown how a conjunct giving of a bed porosity and a flux permits the initialization of a minimization model according to the parameters of the chosen local flux-based model which is comforting for users familiar with such a more traditional approach. However, a same initialization does not mean that the two models will follow the same path, as the minimization-based approach introduces more physics. Indeed, in previous works, we have already shown how our minimization-based formulation can be seen as an Exner equation with a non-local flux (Mohammadi et al. 2011; Bouharguane et al. 2012) with terms similar to those encountered in Fowler-like models (Fowler 2001; Kouakou et al. 2006). Those terms bring the contribution of some non-local physics to the morphodynamics.

This formulation also permits the comparison of the bed ψ evolution predicted minimizing different physical functional $\mathcal{J}$. It is thus a very efficient exploratory model as defined by Murray (2007). However, it is not possible to find the functional $\mathcal{J}$ associated to a given flux q because this requires the mathematical concept of integration with respect to the shape to give sense to:

$$\mathcal{J} = \frac{\Upsilon}{1-\lambda_p}\int_\psi \nabla.q\ d\psi.$$

Unfortunately, unlike differentiation with respect to the shape (Mohammadi et al. 2009), the concept of integration with respect to the shape does not exist as of today.

2.4 Model Constraints

The first constraint Υ takes into account the physical characteristics of the sand and represents the mobility of the sediment. Simulations with varying Υ that reflect variations of the d_{50} grain diameter from 0.25 mm to 2 mm were performed. Changes in the beach profile were observed but no significant alteration of the trends in beach profile evolution through time. The asymptotic behavior of the simulations remains the same although the velocity at which a given profile is reached changes. Further explanation of the nature of the Υ parameter will be given at a later stage of the model development. The second parameter Λ is a local function which represents the influence of the relative water depth kh on the beach profile dynamics and is defined after the term describing the vertical attenuation of the velocity potential according to linear wave theory (R.L. Soulsby 1987):

$$\begin{array}{rccl} \varphi: & \Omega \times [0, h_0] & \longrightarrow & \mathbb{R}^+ \\ & (x, z) & \longmapsto & \dfrac{\cosh(k(x)(h(x) - (h_0 - z)))}{\cosh(k(x)h(x))} \end{array} \tag{1.13}$$

In unconstrained circumstances, for instance, if a total sand volume constraint does not need to be enforced, we set $d = -\nabla_\psi \mathcal{J}$, which indicates a direction for local minimization of $\mathcal{J}$ with regards to ψ. The calculation of $\nabla_\psi \mathcal{J}$ is described in 2. However, constraints are added to the model to incorporate more physics and to deliver more realistic results. While driving forces behind the morphological evolution of the beach profile are described by the minimization of the cost function $\mathcal{J}$, secondary processes are expressed by constraints. In the interest of simplicity, we have adopted two physical constraints though more can be introduced if necessary. The first concerns the local slope of the bottom. Depending on the composition of the sediment, the bottom slope is bounded by a grain-dependent threshold M_{slope} (Dean et al. 2004). This is conveyed by the following constraint on the local bottom slope illustrated by 1.6:

$$\left| \frac{\partial \psi}{\partial x} \right| \leq M_{\text{slope}} \tag{1.14}$$

The dimensionless parameter M_{slope} represents the critical angle of repose of the sediment. This angle is based on observed angles in natural beach environments, which are often between 0.01 and 0.2 (Bascom 1951; Vos et al. 2020; Short 1996). We have considered the observed critical angle of 0.2.

A second example concerns the sand stock in the case of an experimental flume. In a flume, the quantity of sand must be constant over time, as given by (5.24), contrarily to an open-sea configuration where sand can be transported between the nearshore zone and a domain beyond the closure water depth where sediment is lost definitely for beach

morphodynamics (Hattori et al. 1980; Quick 1991). This constraint can be written as :

$$\int_{\Omega} \psi(t,x)\mathrm{d}x = \int_{\Omega} \psi_0(x)\mathrm{d}x \qquad \forall t \in [0, T_f] \tag{1.15}$$

This constraint is necessary for verifying and validating the numerical model with the wave flume experimental data.

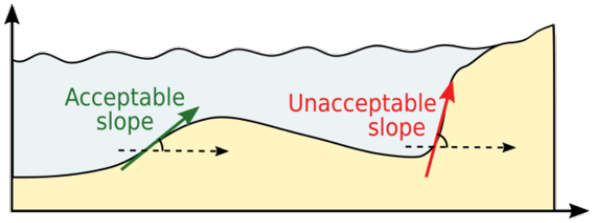

Figure 1.6 – Slope constraint (5.23) from (Cook 2021)

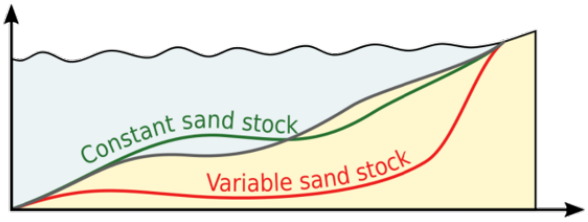

Figure 1.7 – Sand conservation (5.24) from (Cook 2021)

3 Numerical Application

In this section, we present the numerical results produced by the OptiMorph model. For validation purposes, the resulting beach profile is compared to experimental data acquired during a flume experiment. We also conduct a comparative analysis between the beach profiles produced experimentally, by OptiMorph and by XBeach, with the aim of assessing how OptiMorph holds up against existing hydro-morphodynamic models. A brief description of the experiment is provided, as well the as the XBeach model.

3.1 Description of the Experiment

The experimental observations have been collected as part of the COPTER project and a series of laboratory wave-flume experiments were performed in order to investigate the morphodynamic impact of introducing solid geotextile tubes in the nearshore (Bouchette 2017). We use the part of the experiment run without tubes that was devoted to the description of the natural evolution of the beach profile under various wave conditions. Time and length scale ratio are set to $1/3$ and $1/10$ respectively to that of the field.

A flume measuring 36 m long, 0.55 m wide and 1.3 m deep is equipped with a wave-maker and gauges measuring the elevation of the water surface from which wave properties are derived. Artificial particles are placed inside the flume representing the mobile sea bottom and an ultrasonic gauge is used to measure the experimental beach profile. The experimental beach profile, described in Figure 1.1 is subjected to a series of 30-minute storm climates, among which a typical moderate storm event (at the scale of the flume) with a significant wave height and period of $H_s = 135$ mm and $T_s = 2.5$ s.

3.2 XBeach Model

XBeach is an open-source process-based model developed by Deltares, UNESCO-IHE, and Delft University of Technology to simulate the hydro-morphodynamic processes in coastal areas (D. J. Roelvink et al. 2009; Zimmermann et al. 2012; Bugajny et al. 2013; Williams et al. 2015). In brief, XBeach uses four interconnected modules to model near-shore processes (Daly 2009; D. J. Roelvink et al. 2010). The two hydrodynamic modules consist of the short wave module and the flow module. The first is based on wave action equations (Holthuijsen et al. 1989), and incorporates breaking, dissipation (D. J. Roelvink 1993), and wave current interactions, while the latter is governed by shallow water equations (Andrews et al. 1978; Walstra et al. 2000). One of the two morphodynamic modules is the sediment transport module based on the equilibrium sediment concentration equation (Richard Soulsby 1997) and a depth-averaged advection-diffusion equation (Galappatti et al. 1985). The other is the morphology module which concerns seabed transformations such as the evolution of the sea bottom and avalanching.

For the simulations, the domain Ω is defined over 32 m with a uniform subdivision of 320 cells. The incoming wave boundary condition is provided using a JONSWAP wave spectrum (Daly 2009), with a significant wave height of $H_{m0} = 0.015$ m and a peak frequency at $f_p = 0.4$ s^{-1}. The breaker model uses the Roelvink formulation (D. J. Roelvink 1993), with a breaker coefficient of $\gamma = 0.4$, a power $n = 15$, and a wave dissipation coefficient of 0.5. These parameters were calibrated using the hydrodynamic data produced during the physical flume experiment. Concerning sediment parameters, the d_{50} coefficient is set as 0.0006, and the porosity is 2650 kg m^{-3}. No other parameters such as bed friction or vegetation were applied. The model is set to run for a period of 1800 s, as a short-term simulation.

3.3 Hydrodynamic Validation

This section is devoted to the comparison of the two numerical hydrodynamic models to the experimental wave data obtained in the experimental flume of section 3.1. Mean wave height profiles were calculated over the short-term storm simulation, for both Opti-Morph and XBeach, and compared to the mean wave height of the experimental model. The latter was calculated using the measures taken by the gauges of the flume.

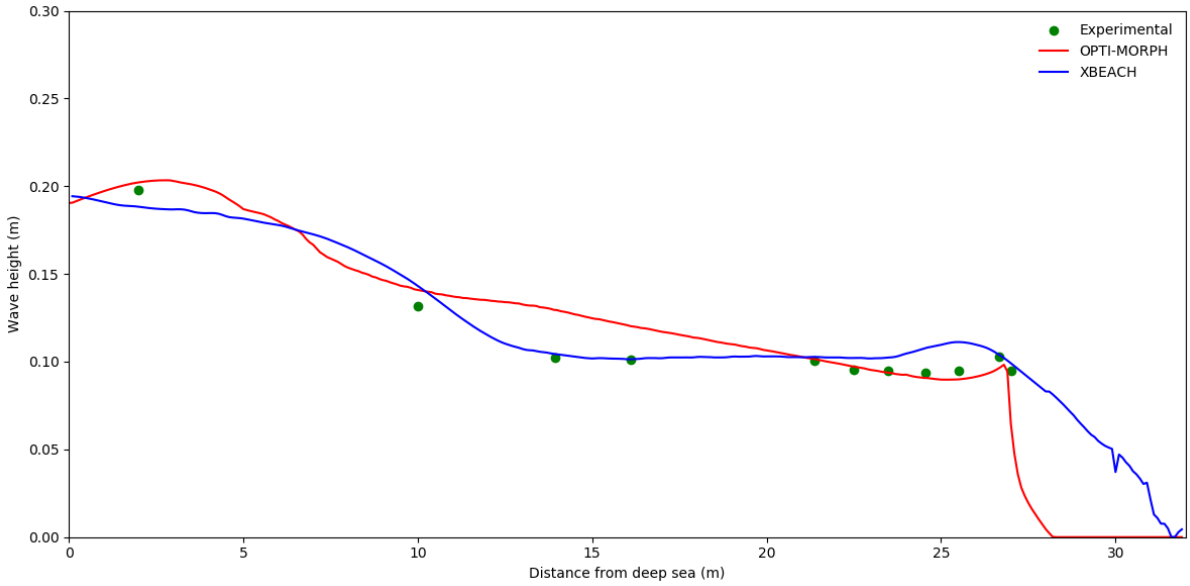

Figure 1.8 – Comparison of mean wave height over a storm simulation. The green points correspond to the mean wave height provided by the gauges of the flume experiment. The mean wave height determined by OptiMorph (red) and XBeach (blue) also appears. The non-zero wave height beyond the shoreline as presented by XBeach is due to wave set-up, which OptiMorph does not handle.

Figure 1.8 shows that the hydrodynamic module of both OptiMorph (red) and XBeach (blue) are both comparable with respect to the experimental measurements (green) excluding, as is often the case, the second point at $x = 6$ m. XBeach demonstrates a close qualitative fit over the 10-22 m section of the flume, whereas OptiMorph excels at the coast (21-27 m), with a near-perfect fit with the experimental data. Despite the simplicity of the hydrodynamic model used by OptiMorph, the resulting wave height is of the same order of magnitude over the cross-shore profile than that measured during the flume experiment, which indicates that the resulting beach profile would be comparable with regard to the forcing energy driving the morphodynamic response.

3.4 Numerical Results of the Morphodynamic Simulations

The OptiMorph model was applied to the configuration of the COPTER experiment of section 3.1, and the resulting beach profile is shown by the red profile, in Figure 1.9.A. The main observation is the decrease of 2.5 cm in height of the sandbar, at $x = 9$ m. We observe a slight lowering of the sea bottom adjacent to the wave-maker, and a slight increase at the plateau, situated at 15-25 m. No mobility is observed at the coast.

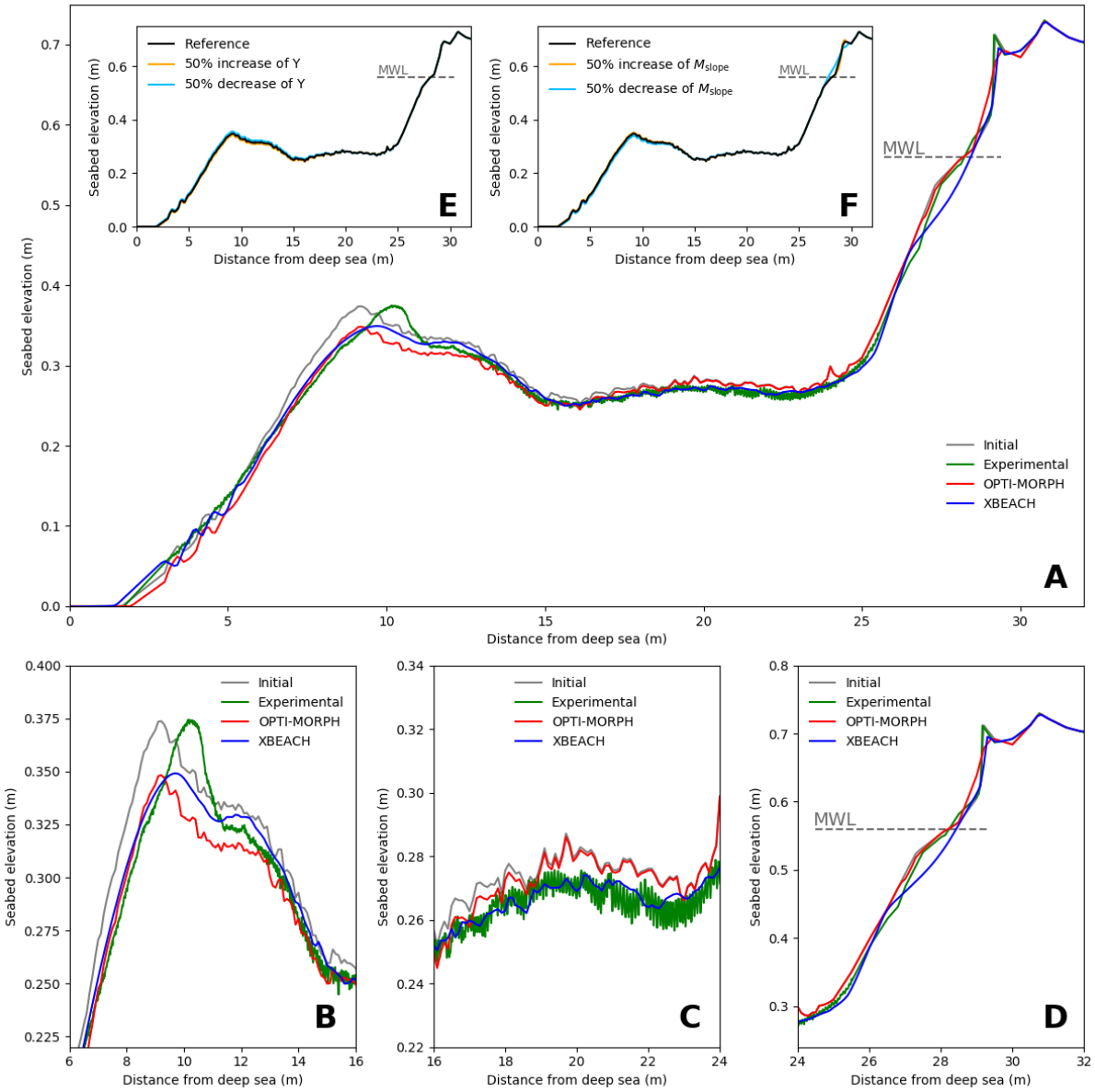

Figure 1.9 – **A.** Results of the numerical simulation calculated over the initial seabed (gray) using the XBeach morphodynamic module (blue) and the OptiMorph model (red). These are compared with the experimental data acquired during the COPTER project (green). The mean water level is denoted MWL and is set at 0.56 m. **B.** Zoomed in view of the sandbar, located between 6 m and 16 m. **C.** Zoomed in view of the plateau, located between 16 m and 24 m. **D.** Zoomed in view at the shoreline, located between 24 m and 32 m. **E.** Robustness analysis of the mobility parameter Y. The reference profile is depicted in black. The orange (resp. light blue) profile is the result of a 50% increase (resp. decrease) in mobility, with all other parameters remaining the same. **F.** Robustness analysis of the maximal sand slope parameter M_{slope}. The reference profile is depicted in black. The orange (resp. light blue) profile is the result of a 50% increase (resp. decrease) of M_{slope} , with all other parameters remaining the same.

When comparing the results provided by OptiMorph (red), with that of XBeach (blue) and the experimental data (green), as shown on Figure 1.9.A, we observe that the red beach profile provided by the OptiMorph model shows a general quantitative agreement

when compared to the experimental data, as does the XBeach morphological module. In fact, both models produce profiles close to the experimental data over the plateau located at 15-25 m from the wave-maker (Fig. 1.9.C). At the shore, OptiMorph matches the experimental data whereas XBeach shows a vertically difference of up to 3 cm at $x = 27$ m (Fig. 1.9.D). Discrepancies on the part of both models occur in the area surrounding the tip of the sandbar, as both OptiMorph and XBeach fail to predict the shoreward shift of the sandbar (Fig. 1.9.B); the experimental data show that the height of the sandbar remains unchanged with regards to the initial profile. Both sandbars have a height of 0.375 m; however, the sandbar resulting from the experimental simulation has moved towards the coast, an occurrence that neither numerical model was able to predict.

As such, this new model based on wave-energy minimization shows potential when compared to XBeach, in the case of short-term simulations.

4 Extension to Multi-1D Simulations

The OptiMorph multi-1D model (Ronan Dupont et al. 2022) is an extension of 1D. It slices a $3D$ bathymetry into n cross-shore transects. They are then launched simultaneously as shown in figure 1.10. They can be run on a classical computer or on a cluster for computation time.

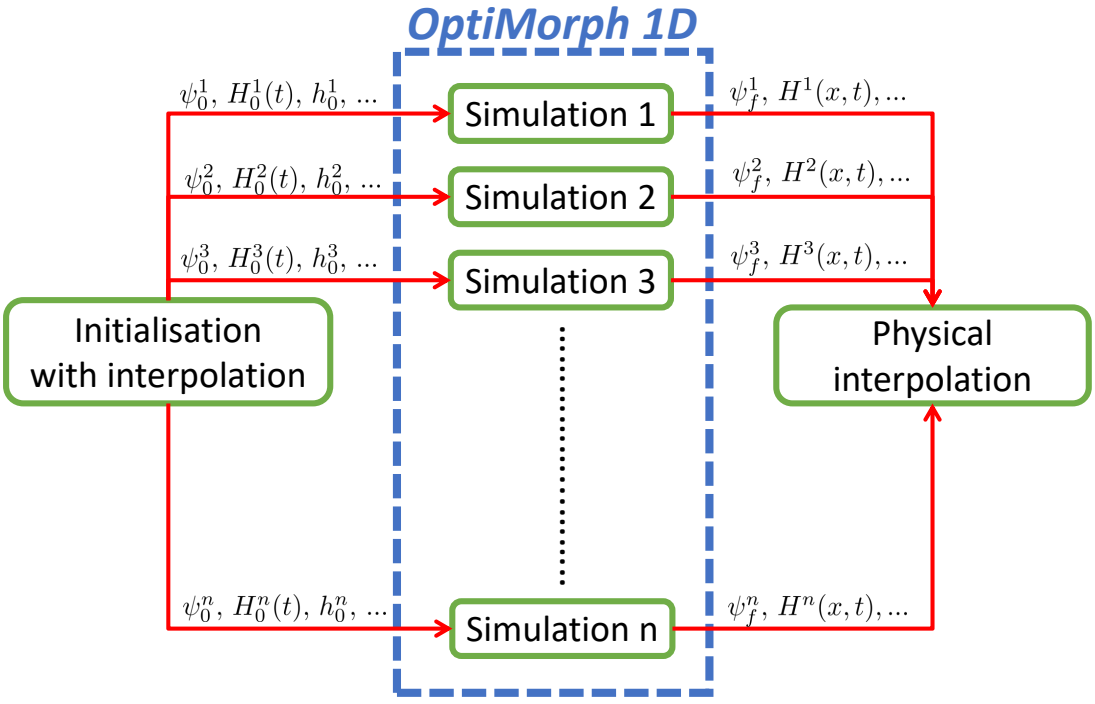

Figure 1.10 – Functional diagram of the multi-1D

Once the n simulations are done, it is essential to link all these simulations by interpo-

lation. This model, the most basic one, has some limitations. Indeed, these simulations assume that all transects have been extracted at locations where there are no long-shore currents. In addition, lateral sandy displacements are not taken into account. In a more advanced version, it could be interesting to take into account these phenomena by adding a source term in the descent equation governing the evolution of ψ.

4.1 Applications to a Multi-1D case near Montpellier

The works of Isèbe et al. (2008b) and Bouharguane et al. (2010) are interested in finding the optimal position of geotextile tubes (protection solutions) on a transverse profile to maximize their effect as a wave attenuator. With this type of approach in mind, we wish to perform a set of multi-1D simulations by placing a geotextile tube on a set of real transverse morphological profiles (Montpellier; Figure 1.11) structure.

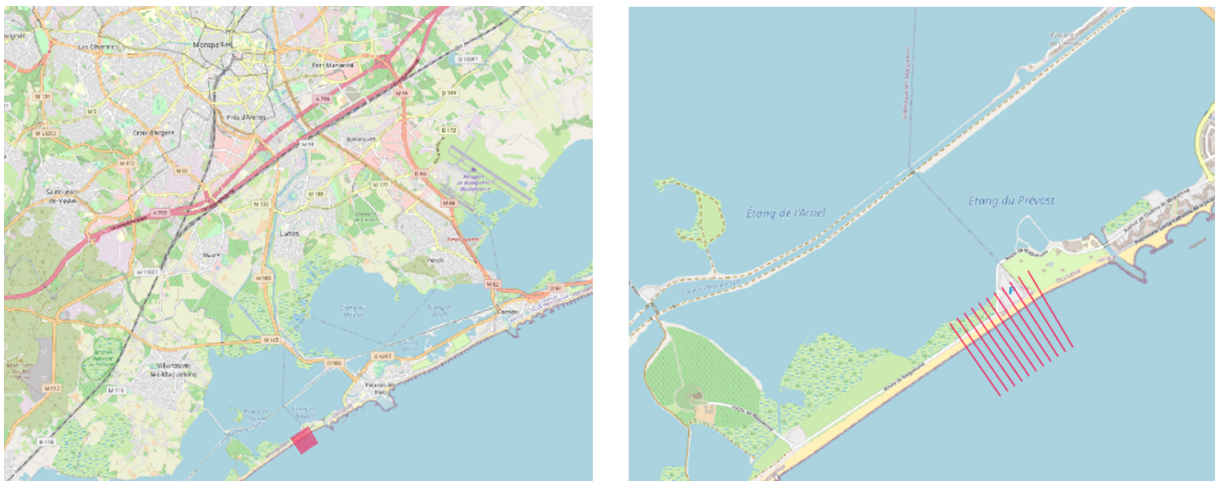

Figure 1.11 – Geography of the simulation near Montpellier

We carry out the simulation of an extreme multi-1D case (on all the profiles); this simulation corresponds to a storm of a few days with waves of a maximum height of $H_{max} = 2\,m$. A geotextile tube is added on the domain in a Gaussian form (whose characteristics vary from one profile to another; figure 1.12.a. Parallelized simulations (HPC computer) are launched and are completed in less than 5 minutes whatever the number of transects (modulo the limit of cores on the cluster). The results are presented in figure 1.12.

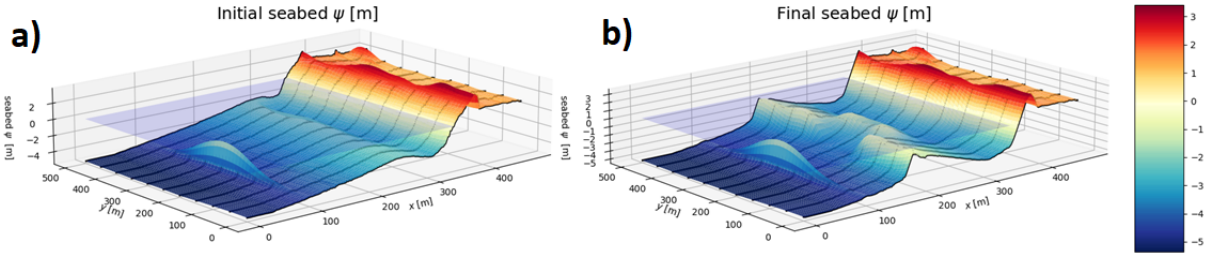

Figure 1.12 – a) Initial sea bottom on the Gulf of Aigues-Mortes by adding a Gaussian geotube with a maximum height of 3m. b) Final bathymetry after a simulation of a storm of several days.

The results show the formation of a pit at the back of the highest and thickest part of the geotextile tube. These results are encouraging as they are very similar to those found in the COPTER experimental campaign (Bouchette 2017) conducted in 2017 in a 3D wave basin (moving bottom).

5 Discussion

5.1 Robustness Analysis of the Consistency in Time and Space of the Morphodynamic model

We computed a reference OptiMorph simulation using a very small coupling time of 0.05 s which is much smaller than what is usually used in hydro-morphodynamic simulations. The simulation was performed with the original bathymetric profile of the COPTER experiment and the forcing of the wave maker.

This simulation provides a reference computed sea bed $\psi_{ref}(T_f, x)$ at some given time T_f. We would like to see the convergence toward this reference solution of various other OptiMorph simulations with different decreasing time steps. From this series of simulations, we quantify a residual error with L^2 norms as $\mathcal{E}_{L^2} = ||\psi_{ref} - \psi||_{L^2}$ in m. We performed 10 simulations with time steps ranging in $[0.05; 160]$ s and we get the results described in figure 1.13.a).

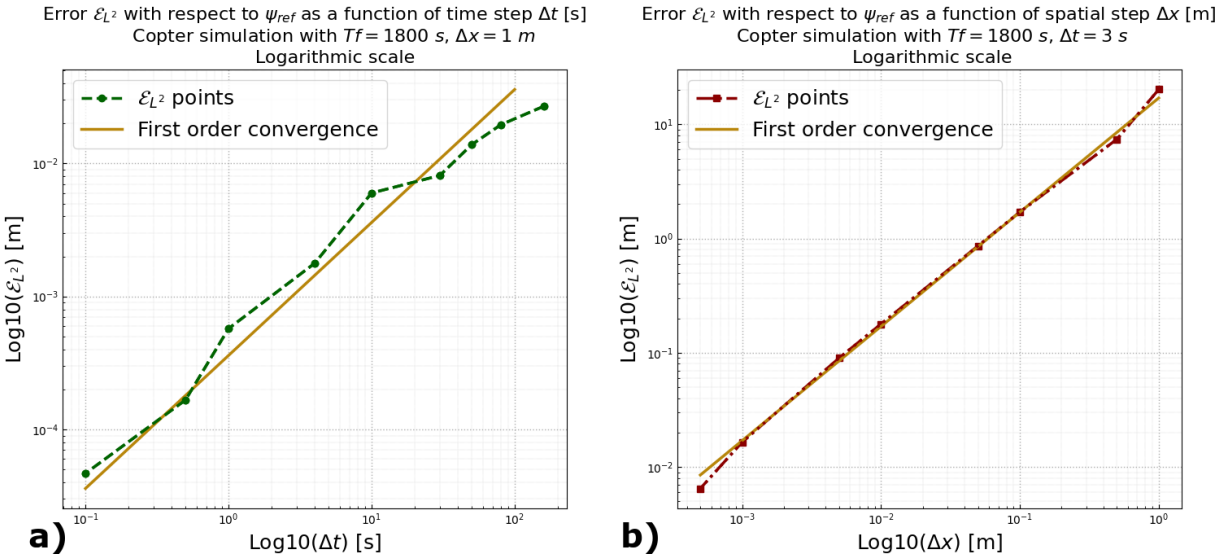

Figure 1.13 – a) Errors $\mathcal{E}_{L^2}$ (green) obtained by simulations of 10 different time steps compared to the reference simulation corresponding to a coupling time of 0.05 s. First order convergence (yellow). b) Errors $\mathcal{E}_{L^2}$ (red) obtained by simulations of 10 different spatial steps compared to the reference simulation corresponding to a spatial step of 0.0002 m. First order convergence (yellow).

In order to analyse the convergences in space and time, we choose, respectively, a reference coupling time of $T_{coupl} = 3$ s and a spatial step size $\Delta x = 1$ m. $T_{coupl} = 3$ s corresponds to the kind of time steps we would like to use in simulations. But, we will use larger spatial resolution in practice. The results in figure **1.13** shows first order (illustrated by the continuous line) convergence rates in both time and space.

To understand why a coupling time of 3 seconds is interesting for computing efficiency, it is useful to look at the CFL stability condition analysis for the shallow-Water model (Marche et al. 2007). The analysis provides a typical upper bound for the time step of the form:

$$\Delta t = \min_i \left(\frac{\Delta x}{2 \max_i (|u_i \pm \sqrt{g h_i}|)} \right) = \frac{\Delta x}{2 \max_i (|u_0 \pm \sqrt{g h_0}|)},$$

where subscript i indicates the mesh node which means that the minimum is taken over all the nodes of the mesh. In our situation, it corresponds to the off-shore position (subscript $i = 0$). Typical values in our simulation are: $u_0 = 10$ m s^{-1}, $\Delta x = 1$ m, $h = 0.55$ m and $g = 9.81$ m s^{-2}. This gives us $\Delta t = 0.04$ s, which is about two orders of magnitude smaller than our reference time step of $\Delta t = 3$ s. In addition, the costs of one iteration of the Shallow-Water and OptiMorph models are comparable.

5.2 The Robustness of the Domain Length

An important step in the analysis of the numerical behavior of the model is the validation of its behavior with respect to the characteristics of the domain and with respect to the forcing. In this part, we are particularly interested in the comparison of simulations of the morphodynamic evolution for identical forcing but different domains. A multi-day storm is studied by varying the length of the domain while keeping the same linear range of slope 1e-2. The results obtained are presented in Figure 1.14.b and show the formation of a realistic stable bar for domain lengths in the interval [600, 1200, 1800, 3000] m.

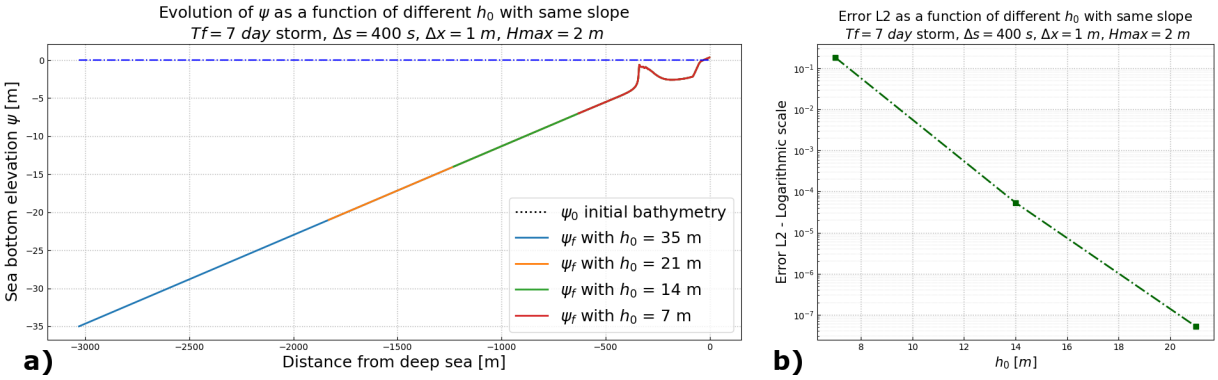

Figure 1.14 – a) Different final bottom profiles for domains of sizes [600, 1200, 1800, 3000]m corresponding to offshore water heights of h= [7, 14, 21, 35] m. The representation is truncated at 7 m depth. b) L^2 error comparing each simulation to the reference solution corresponding to the 3000 m domain (the longest, represents deep water conditions).

Figure 1.14.b shows the convergence of the solution as a function of the change in domain length. As for the convergence on spatial resolution, we consider a reference simulation which is that of a domain of length 3000 m. The observed convergence thus ensures that regardless of the domain size, the shallow water swell transition always occurs at the same point and the morphodynamic response occurs in the same way.

5.3 Parameter Robustness Analysis

One of the advantages of the OptiMorph model is the low number of morphodynamic hyper-parameters required. At the present time, OptiMorph requires two hyper-parameters: the mobility parameter Υ and the maximal slope parameter M_{slope}. Here, an assessment on these parameters is conducted. In Figure 1.9.E, three simulations were performed in identical settings with changes made solely to the mobility parameter. Initially, this parameter Υ has a value of 5×10^{-6} m s kg^{-1}. Figure 1.9.E shows no significant difference despite a 50% increase ($\Upsilon = 7.5 \times 10^{-6}$ m s kg^{-1}) (orange) or decrease ($\Upsilon = 2.5 \times 10^{-6}$ m s kg^{-1}) (light blue) of Υ with regard to the baseline beach profile (black). Similar conclusion can be deduced for the maximal slope parameter M_{slope}, whose reference value here is 0.2. The corresponding parameter of XBeach is *wetslp*,

described in the XBeach manual as the critical avalanching slope under water, and is also set to 0.2. In Figure 1.9.F, we observe little difference between the reference seabed (black), the seabed resulting from a 50% increase ($M_{\text{slope}} = 0.3$) (orange) and the seabed resulting from a 50% decrease ($M_{\text{slope}} = 0.1$) (light blue). The only apparent discrepancy can be found at $x = 28$ m, where the bottom slope is at its steepest, and therefore the sand slope constraint is more prone to be active. The reduction of the critical angle of repose results naturally in a less steep slope. The robustness of OptiMorph in relation to both the mobility parameter and the slope parameter, despite a significant increase or decrease of their value, is apparent. Further simulations show that the robustness of these parameters is not specific to this particular flume configuration, but can be observed regardless of the initial configuration.

5.4 Mid-term Simulations

This section is devoted to a medium term behavior of OptiMorph, the main question being, is this numerical model capable of creating an equilibrium state after being subjected to a great number of repeated events. Five forcing scenarios, lasting either 2 or 6 days, were applied to the same initial seabed in the same parametric configuration. The current OptiMorph code is in Python. Typically, using time-steps of 1 s simulating a day of forcing requires about 1.5 hours on a 2GHz PC computer. Each time iteration gathering the steps presented in this chapter requires therefore about 63 ms. Regarding the section 5.1, we could use 3 s time-step and divide the simulation time by 3. An analysis of the resulting beach profiles is performed as well as their behavior throughout the simulation. The latter is achieved through a comparative study of four time-series, focusing on: (1), the vertical evolution of bottom elevation at the tip of the sandbar; (2), the vertical evolution of bottom elevation at a point of the plateau; (3), the distance between the wave-maker and the onset of the sea bottom; and (4), the location of the shoreline position.

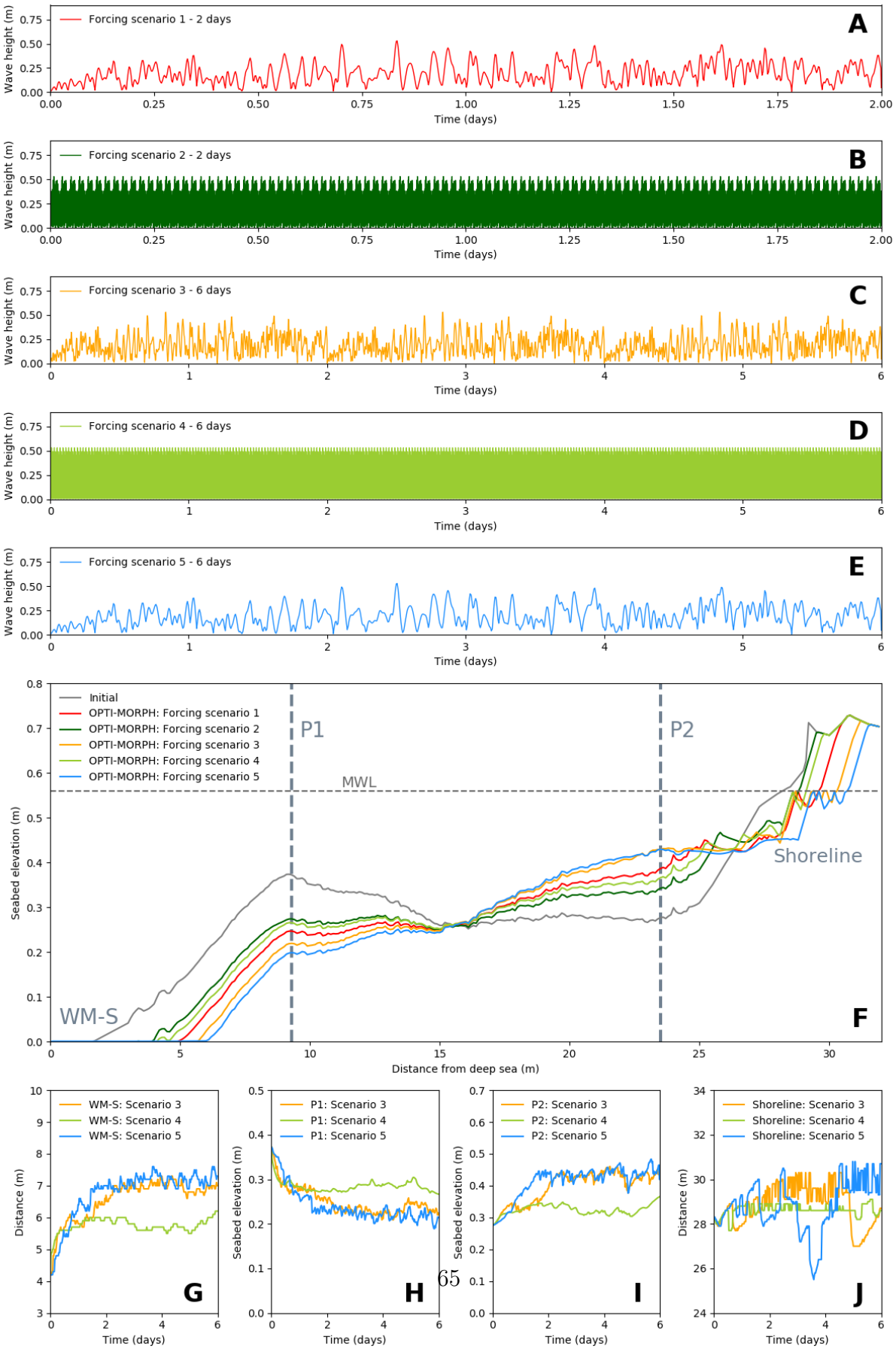
Forcing scenario 1 - 2 days
A
Forcing scenario 2 - 2 days
B
Forcing scenario 3 - 6 days
C
Forcing scenario 4 - 6 days
D
Forcing scenario 5 - 6 days
E
Wave height (m)
Time (days)
Initial
OPTI-MORPH: Forcing scenario 1
OPTI-MORPH: Forcing scenario 2
OPTI-MORPH: Forcing scenario 3
OPTI-MORPH: Forcing scenario 4
OPTI-MORPH: Forcing scenario 5
P1
P2
MWL
Shoreline
WM-S
F
Seabed elevation (m)
Distance from deep sea (m)
WM-S: Scenario 3
WM-S: Scenario 4
WM-S: Scenario 5
G
Distance (m)
P1: Scenario 3
P1: Scenario 4
P1: Scenario 5
H
P2: Scenario 3
P2: Scenario 4
P2: Scenario 5
I
Shoreline: Scenario 3
Shoreline: Scenario 4
Shoreline: Scenario 5
J

Figure 1.15 – Mid-term simulation of OptiMorph. **A.** Forcing wave height for scenario 1, composed of several mid-term events over a 2-day period. **B.** Forcing wave height for scenario 2, composed of numerous short-term events over a 2-day period. **C.** Forcing wave height for scenario 3, composed of several mid-term events over a 6-day period. **D.** Forcing wave height for scenario 4, composed of numerous short-term events over a 6-day period. **E.** Forcing wave height for scenario 5, composed of few mid-term events over a 6-day period. **F.** Seabeds resulting from the different forcing scenarios produced by OptiMorph. Two points of interest have be identified: P1 located at $x = 9.3$ m and P2 located at $x = 20.1$ m. **G.** Evolution of the distance, devoid of sediment, between the wave-maker (located at $x = 0$ m) and the seabed (WM-S), regarding forcing scenarios 3, 4, and 5. **H.** Vertical evolution of seabed elevation at P1, driven by the 6-day forcing scenarios 3, 4, and 5. **I.** Vertical evolution of seabed elevation at P2, driven by the 6-day forcing scenarios 3, 4, and 5. **J.** Evolution of shoreline position, driven by the 6-day forcing scenarios 3, 4, and 5.

Applying OptiMorph over a longer time-series leads to the results of Figure 1.15. The two 2-day forcing scenarios are shown in Figures 1.15.A and 1.15.B. In both cases, we observe that the resulting beach profiles in Figure 1.15.F are subjected to the destruction of the sandbar and have a tendency to evolve progressively towards an equilibrium beach profile (Engineers 2002). Simulations over a 6-day period were conducted to confirm this tendency. These scenarios are depicted in Figures 1.15.C, 1.15.D, and 1.15.E; the resulting profiles given in Figure 1.15.F show once again the destruction of the sandbar, the elevation of the plateau, and some erosion at the shoreline. Furthermore, all three tend towards an equilibrium state. This is confirmed by the four time-series analysis presented in Figures 1.15.G, 1.15.H, 1.15.I, and 1.15.J. The vertical elevation of the seabed at both points P1 and P2 show initial variations over the first 2 days: a decrease in the case of P1 (cf. Figure 1.15.H) and an increase in the case of P2 (cf. Figure 1.15.I). However, both studies show a stabilization of the sea bottom elevation over the last 4 days of the 6-day period. Similar conclusions can be drawn regarding the length of the zone containing no sediment adjacent to the wave-maker (cf. Figure 1.15.G). An initial increase between 2 and 3 meters can be observed, with stability achieved in the later stages of the simulations. Finally, Figure 1.15.J shows the evolution of the shoreline position. Initially found at $x = 28.3$ m, all scenarios provoke a retreat of the shoreline: 0.4 m in scenario 3, 0.3 m in scenario 4, and 2 m in scenario 5. The shorelines of the latter two converge, whereas scenario 3 shows an abrupt advance of the shoreline at day 5, with an attempt to return back to its stable state of $x = 30$ m. The seabed has been flattened, the sandbar has been destroyed and erosion can be observed at the coast (Grasso et al. 2011). This tendency to evolve towards an equilibrium state (Dean et al. 2004) is consistent with the choice of morphogenic and constant storm-like forcing conditions.

The comparisons made between the two 2-day simulations and the three 6-day simulations, in this quite limited configuration, also reveal the little influence heritage has on the morphodynamic response. Both scenarios 1 and 2 have a comparable cumulative incoming wave energy density $E_H = \frac{1}{16}\int_0^T \rho g H_0^2 \mathrm{d}t$ of 0.0591 J m^{-2}. The resulting beach profiles evolve towards similar profiles (reduction of the sandbar, increase of elevation of the plateau, and erosion at the coast), despite two different forcing conditions. Similar conclusions can be drawn regarding the 6-day simulations, where the cumulative energy

density of all three is equal to 0.177 J m^{-2}.

6 Conclusions

OptiMorph shows potential as a fast, robust, and low complexity morphodynamic model involving only two hyper-parameters. Despite using a basic hydrodynamic model for the description of the complex coupling of hydrodynamic and morphodynamic processes, we can nevertheless observe that a numerical model based on an optimization theory works effectively, with comparable results to a state of the art hydro-morphodynamic model requiring the tuning of dozens of hyper-parameters. Mid-term simulations also show typical morphodynamic behavior, with the tendency of the seabed to evolve towards an equilibrium state. Moreover, the results of the multi-1D code are very encouraging. These results demonstrate the tremendous potential of OptiMorph, a constrained energy minimization morphodynamic model.

Chapter key points

- A fast, robust, low-complixity morphodynamic model based on the minimization principle.
- Valid comparisons with well-known morphodynamic software such as XBeach.
- Results showing a long-term equilibrium solution.
- A numerical validation has been done (time, space and domain length convergence).
- An extension to Multi-1D has been tested on a case off Montpellier.
- A strong constraint in the choice of the hydrodynamic model which must be analytically differentiated.